Atomistic simulations of a helium bubble in silicon carbide

Laurent Pizzagalli, M.-L. David

Atomistic simulations of a helium bubble in silicon carbide

L. Pizzagalli[a,*], M.-L. David[a]

[a]*Institut P′, CNRS UPR 3346, Université de Poitiers, SP2MI, Boulevard Marie et Pierre Curie, TSA 41123, 86073 Poitiers Cedex 9, France*

Abstract

Large scale molecular dynamics calculations have been carried out to investigate the properties of nanometric helium bubbles in silicon carbide as a function of helium density and temperature. A dedicated interatomic potential has been developed to describe the interactions between helium and SiC atoms. The simulations revealed that the helium density cannot exceed a certain threshold value, which depends on temperature, because of the plastic deformation of the SiC matrix. Both local amorphization at low temperatures, and nucleation and propagation of dislocations at high temperatures, have been identified as activated plasticity mechanisms. This work also predicts that very high pressure, up to 60 GPa could be reached in helium bubbles in silicon carbide.

Keywords: Silicon carbide, Helium bubbles, Plasticity, Molecular dynamics calculations

1. Introduction

Silicon carbide (SiC) has attracted a lot of attention in the last decades because of its excellent thermal, chemical, electronic, and mechanical properties [1, 2], which makes it a suitable candidate for applications in several domains. In a nuclear fission context, SiC can be used as a fuel cladding material. It has also a great potential in future fusion reactors, as structural material. In both cases, SiC is exposed to high-radiation environments, and to the accumulation of nuclear reaction products among which helium. Such a context also pertain to astrophysics, since silicon carbide is a significant constituant of interstellar dust grains [3]. Helium can be produced in the burning shells of late-stage stars, and trapped in these grains.

As a quasi inert element, helium tends to aggregate in most materials, ultimately forming large extended defects like bubbles or platelets. Depending on the conditions, large pressures can be present in those defects. It is especially the case for high dose rates of incoming helium atoms combined with a restricted vacancy supply. In silicon carbide, several studies reported observations of helium-filled bubbles and platelets [4–12]. Such highly pressurized defects can significantly degrade the structural integrity of the host, a particularly annoying feature for a structural or confining material.

Mechanisms leading to bubble formation have been extensively investigated, in particular for metals [13–15] and few other materials like silicon [16–18] or uranium dioxide [19]. However, most of available studies for silicon carbide concern the first stages of bubble formation, and in particular the stability and migration properties of a single embedded helium atom [20–28], as well as interactions between helium atoms or between helium and a vacancies cluster [7, 29–32]. Little is known on the properties of full grown spherical helium bubbles in silicon carbide. To our knowledge, the sole contribution to this issue was made by Couet and co-workers, who examined the influence of temperature on helium content [33]. Nevertheless, only small nanocavities were considered in this work, with diameters less than 1 nm. The lack of information for larger helium-filled bubbles clearly calls for additional studies.

Furthermore, recent investigations in our group based on spatially resolved electron energy-loss spectroscopy in transmission electron microscopy experiments revealed that very high helium densities, ranging from 120 to 200 He nm^{-3}, can be obtained for bubbles in silicon [34, 35]. Such values largely exceed predictions coming from the well known Laplace-Young relation. Also, atomistic simulations show that the bubble internal pressure has a significant impact on the silicon matrix, which yield by amorphization [34]. New measurements hint that even higher helium densities, in the 150–220 He nm^{-3} range, could be achieved for silicon carbide [36]. It is then necessary to examine whether similar or different plasticity mechanisms than in silicon are activated to sustain the pressure associated with the bubbles.

In this paper, the results of molecular dynamics calculations of helium-filled bubbles in 3C silicon carbide are presented and discussed. Our work is focused on the influence of the helium density on the bubble properties, and additionally on the state of the SiC matrix. In the next section, the details of the calculations are provided. Next, the results and the analysis of the plastic relaxation mechanisms are presented in two separate sections.

2. Numerical simulations procedure

The molecular dynamics calculations were performed using the code LAMMPS [37], and a timestep of 1 fs for integration of motion equations. The classical potentials modeling the in-

*Corresponding author

Email addresses: Laurent.Pizzagalli@univ-poitiers.fr (L. Pizzagalli), Marie-Laure.David@univ-poitiers.fr (M.-L. David)

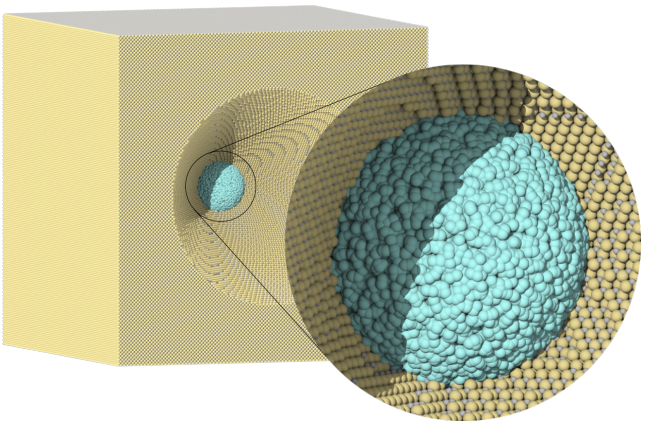

Figure 1: Model of an helium filled bubble embedded in cubic silicon carbide, before molecular dynamics calculations. Some portion of Si and C atoms were removed for a better view.

teraction between Si, C, and He atoms are described in the Appendix A.

Models of a helium bubble in silicon carbide are generated according to the following procedure. A large cubic silicon carbide bulk, with a lattice parameter $a_0 = 4.3593273$ Å, is first created. The dimensions along canonical directions are equal to 39.23 nm, equating to about 5.8 million atoms. Next a spherical cavity is carved in the center, with a diameter of 6.5 nm, in which helium atoms are randomly introduced (Fig. 1). The helium density is expressed as the number of He atoms in a Si+C elementary volume V = 20.7109 Å^3, as is customary in the literature. We considered He/V initial density values in the range 1–12.

For each He/V value, the following procedure is applied. First, a 0.1 ps run in the NVE ensemble is carried out, with atomic displacements limited to at most 0.1 Å at each step. This ensures to separate strongly overlapping atoms. Second, a conjugate gradient minimization is performed to obtain the system state at 0 K. Then four molecular dynamics runs in the NVT ensemble are carried out in succession, with the following temperatures (durations): 10 K (50 ps), 300 K (60 ps), 600 K (70 ps), and 900 K (80 ps). Note that for each temperature, the supercell dimensions are scaled to avoid thermal stress buildup. The $a_0(T)$ values, determined from independent molecular dynamics, are 4.35958 Å (10 K), 4.36756 Å (300 K), 4.38036 Å (600 K), and 4.39490 Å (900 K).

For each temperature, various quantities are monitored and averaged once thermalization is achieved. It concerns in particular the atomic stress tensors $\sigma^i_{\alpha\beta}$, as implemented in LAMMPS [37], using the Voronoi atomic volume V_i. This last quantity allows for determining the bubble volume and the helium density. For further analysis, we also computed the pressure p and von Mises stress σ_{vm} for each atom according to

$$p = \frac{\sigma_{xx} + \sigma_{yy} + \sigma_{zz}}{3} \qquad (1)$$

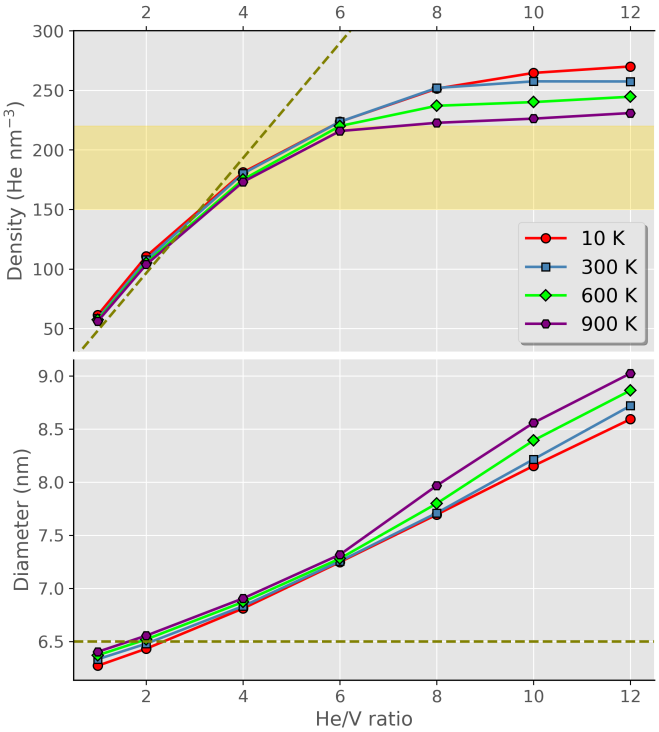

Figure 2: Calculated helium density in the bubble (top) and bubble diameter (bottom) versus initial He/V ratio, for different temperatures (10 K: red circles, 300 K: steelblue squares, 600 K: green diamonds, 900 K: purple hexagons). The dashed olive lines show the density equivalent to the initial He/V ratio (top), and the initial diameter (bottom). The yellow area corresponds to the range of measured helium density values in SiC for bubbles of similar diameter [36].

$$\sigma_{vm} = \frac{1}{\sqrt{2}}\left[(\sigma_{xx}-\sigma_{yy})^2 + (\sigma_{yy}-\sigma_{zz})^2 + (\sigma_{zz}-\sigma_{xx})^2 + 6\left(\sigma^2_{xy}+\sigma^2_{xz}+\sigma^2_{yz}\right)\right]^{1/2} \qquad (2)$$

3. Results

The analysis of the final structures for each temperature and He/V value shows that all helium atoms remain in a quasi-spherical cavity for He/V ratios equal or lower than 4. For higher values, either few helium atoms are found to be located in interstitial positions in SiC, or the bubble loses its spherical shape as a result of plastic yielding of the matrix. These mechanisms will be described in details in the next section.

Because of this issue, there is no easy way to unambiguously determine quantities like volume or diameter of the bubble. As in previous works [34, 38, 39], the bubble volume is here calculated as the sum of helium Voronoi volumes, from which a diameter is obtained by assuming a spherical shape. Consequently, the bubble volume is slightly underestimated for low He/V ratios, because of the presence of a gap at the He–matrix interface [34, 40]. On the contrary, at high He/V ratios, the volume is slightly overestimated, by less than 1 % typically, because of the interstitial heliums. For the same reasons, one

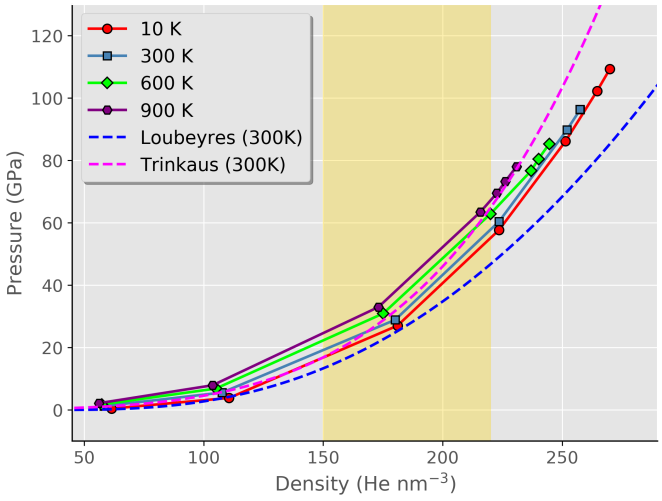

Figure 3: Calculated pressure inside the bubble as a function of the calculated helium density, for different temperatures (10 K: red circles, 300 K: steelblue squares, 600 K: green diamonds, 900 K: purple hexagons). The dashed blue and magenta lines show the pressure versus density variations at 300 K given by the equation of states of Loubeyres et al. [42], and Trinkaus [13], respectively. The yellow area corresponds to the range of measured helium density values in SiC for bubbles of similar diameter [36].

should be cautious regarding the determination of helium density and pressure in the bubble. In this work, the helium density is calculated as the ratio of the number of helium atoms included in a sphere of diameter 2 nm centered on the bubble, over the sum of their Voronoi volumes. The internal pressure is next computed as an average over these atoms. This choice obviates the aforementioned issue, and allows for a meaningful comparison with experiments where helium density is measured in the center of bubbles [41].

The helium density as a function of the He/V ratio and temperature is shown in Fig. 2. These curves resemble those calculated for an helium bubble in a silicon matrix [34]. For low He/V ratios the final density increases like the initial one, with little influence of the temperature. However, for He/V > 2, the slope of the density curves decreases, until a plateau is seemingly reached at the highest He/V ratios. In this regime, the highest the temperature, the lowest the maximum density. Note that this behavior is not specific to silicon carbide, since previous computational investigations led to similar conclusions in iron [38] or uranium dioxide [19], for instance. Since almost all helium atoms remain in the bubble, these variations are evidently caused by the increase of the diameter with the He/V ratio, as seen in Fig. 2, bottom graph. For He/V < 6, the SiC matrix is elastically deformed, with little influence of temperature. Conversely, at higher ratios, the diameter is significantly dependent on temperature, hinting that plastic deformation occurred.

The helium density in bubbles depends on irradiation conditions, and a wide range of values is doubtless possible. Until recently, no experimental data were available for silicon carbide. Our own investigations yield helium densities in the range 150–220 He nm^{-3} at 300 K, for 4–7 nm diameter bubbles [36]. In the present simulations, such values correspond to initial He /V ratios equal to 4–6. However, high temperature annealing up to 1673 K was performed to form these bubbles, which would indicate that our systems with higher He/V ratio could also be representative of the experiments. In fact, the extrapolation of the data presented in Fig. 2 to temperatures higher than 900 K suggests that the threshold helium density could be lower than 220 He nm^{-3}, even for a He/V ratio greater than 6.

Figure 3 shows the computed helium pressure as a function of the density, in the center of the bubble, for the different temperatures. The pressure is obviously proportional to the density and to the temperature. Therefore, the largest pressures are reached for the highest helium densities, or, for the highest temperatures (for a given density value).

We compare our results at 300 K to pressures given by two validated equation of states (EOS). One has been proposed by Trinkaus and has been largely employed for helium-filled bubbles [13]. The other is appropriate to describe helium for high density [42]. One can see in Fig. 3 that the Trinkaus EOS yields higher pressure than the other one, and that the difference tends to increase as a function of the density. Furthermore, our computed pressure values fall in between those two EOS. Note that recent investigations highlighted the influence on pressure of the interaction between matrix and helium atoms, stressing the need to redefine the EOS for helium in bubbles [19, 43–46]. However, this effect is especially important for small bubbles with diameters 1–2 nm, i.e. much smaller than in the present work. This explains why our computed helium pressure is in good agreement with available bulk helium EOS.

These curves also tell us that the measured density range of 150–220 He nm^{-3} corresponds to pressures ranging approximately from 20 to 60 GPa, i.e. much higher than usually found for helium bubbles in metals [47, 48], or than predicted using the Laplace-Young relation. Note that we observed a similar situation in silicon [34].

4. SiC matrix analysis

In this section, we report our analyses on the state of the SiC matrix in relation with the temperature and the helium density in the bubble. The volume variations shown in Fig. 2 suggest that the matrix is elastically deformed for He/V ratios lower than 6 (equivalent to a final density lower than 220 He nm^{-3}), and plastically deformed beyond. To substantiate this hypothesis, an in-depth analysis is required. First, we used the polyhedral template matching (PTM) method [49] to identify the crystalline environment of the Si/C atoms. This method is particularly suited in our case, because it is efficient even in case of significant thermal vibrations or elastic distortions. The crystalline environment of Si/C atoms is essentially cubic zinc blende, with very small amounts of hexagonal zinc blende for high density and temperature cases. Furthermore, we found a non negligible proportion of unidentified atoms, i.e. in a locally disordered environment. Amorphization in the vicinity of the matrix-bubble interface was shown to be the favored plasticity mechanisms in the case of helium bubbles in silicon [34]. Second, a dislocation extraction analysis (DXA) [50] is carried out, to determine

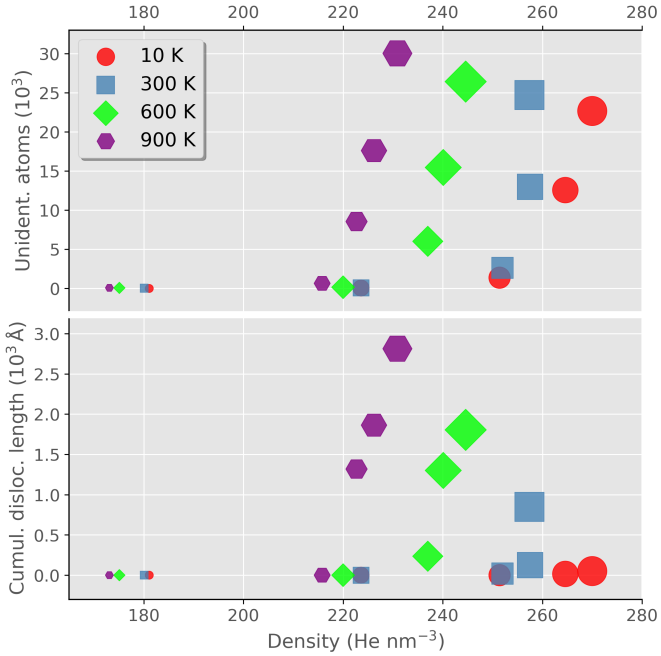

Figure 4: Numbers of Si/C atoms in an unidentified environment (i.e. not cubic or hexagonal zinc blende) (top), and cumulative dislocation length (bottom) as a function of the helium density in the bubble (in He nm^{-3}), for different temperatures (10 K: red circles, 300 K: steelblue squares, 600 K: green diamonds, 900 K: purple hexagons). The symbol size is proportional to the initial He/V ratio. These quantities are calculated using the polyedral template matching method [49], and the dislocation extraction analysis tool [50] as implemented in Ovito [51].

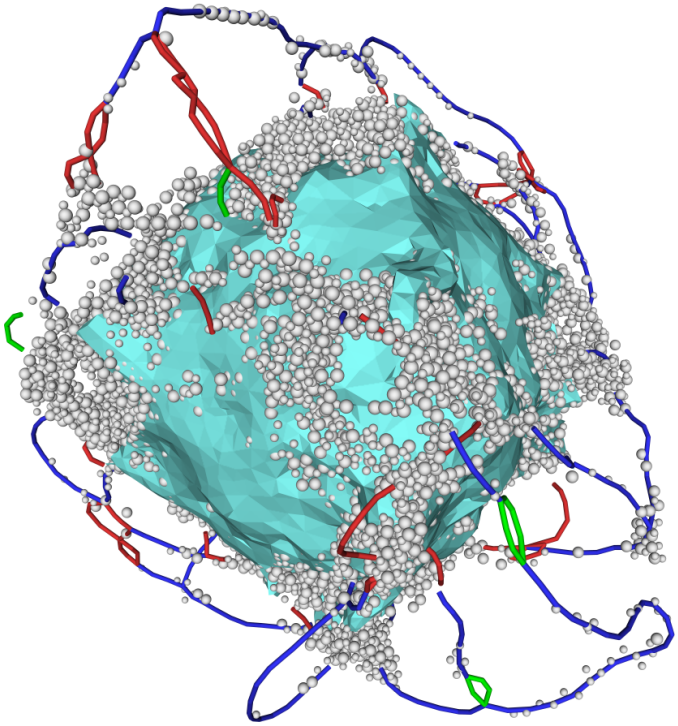

Figure 5: Plastic deformation around an helium-filled bubble with He/V = 10, at 900 K. The cyan meshed surface is computed so as to contain all helium atoms [52], and thus allows for a rough estimate of the bubble shape. Also represented as small shite spheres are Si/C atoms which are not in a cubic or hexagonal zinc blende environment, according to the algorithm depicted in [53]. Finally, the colored thin tubes show dislocation lines identified using DXA [50]. Blue lines are perfect dislocations with Burgers vector 1/2⟨110⟩, green lines partial dislocations with Burgers vector 1/6⟨112⟩, whereas red lines correspond to unidentified dislocations.

whether plastic deformation by dislocation loop punching occurred.

The results presented in Fig. 4 corroborate our primary conclusions. In fact, for helium densities up to 215–225 He nm^{-3}, all atoms remain in a crystalline environment and no dislocations are detected. We observe the onset of plastic deformation of the SiC matrix above this threshold. This confirms the purely elastic deformation of the SiC matrix, at least for He/V value lower or equal to 6. Increasing the initial He/V ratio, and thus the applied stress in the matrix, and/or the thermal activation lead to an increase of both the amount of unidentified atoms and punched dislocation loops. However, the dependences on stress and temperature are markedly different between the two mechanisms. At the lowest temperature, i.e. 10 K, only amorphization occurs, with no nucleated dislocations (red circles in Fig. 4). These conditions correspond to the highest helium densities attained in the simulations. Fig. 4 also reveals that the disorder increases significantly with the applied stress, but little with temperature. Conversely the temperature has a strong influence on dislocation loop punching, with a large increase of cumulative dislocation length for a given initial He/V ratio.

An example of configuration obtained after substantial plastic relaxation at high temperature and initial He/V ratio, is shown in the Fig. 5. The meshed surface is built so as to include all helium atoms. Its initially spherical shape is lost after relaxation in these conditions, with helium atoms expanding in various directions. Those seem to be mostly ⟨100⟩, although it is hard to be conclusive. A less ambiguous point is the spatial correlation between helium protrusions and clusters of disordered atoms, represented as white spheres. It proves that the SiC matrix yields by amorphization at different locations because of the pressure exerted by helium atoms.

For high temperatures and densities cases, the DXA technique identified dislocation loops near the helium bubble (see Figure 5). Hereinafter, we restrict our discussion at a qualitative level, since there are several factors which can complicate the DXA analysis. In fact, the zoology of dislocations in cubic diamond and zinc-blende lattices is notoriously complicated [54, 55]. Furthermore, disorder, structurally or due to temperature, as well as a significant stress gradient, are present in the vicinity of the bubble. This probably explains why several dislocations are not formally identified by DXA (red lines in Fig. 5). Most of the dislocations are non dissociated with Burgers vector 1/2⟨110⟩, with half-loop shapes connected to the bubble-matrix interface. They are located in {111} planes. Such dislocations are typical of the deformation of silicon carbide for temperatures below the brittle to ductile transition [54, 56]. In few locations, we observe dissociation of the dislocation line in 1/6⟨112⟩ partial dislocations. The length of dissociated segments seem to increase with the temperature, in agreement with the proven fact that at high temperature, plastic deforma-

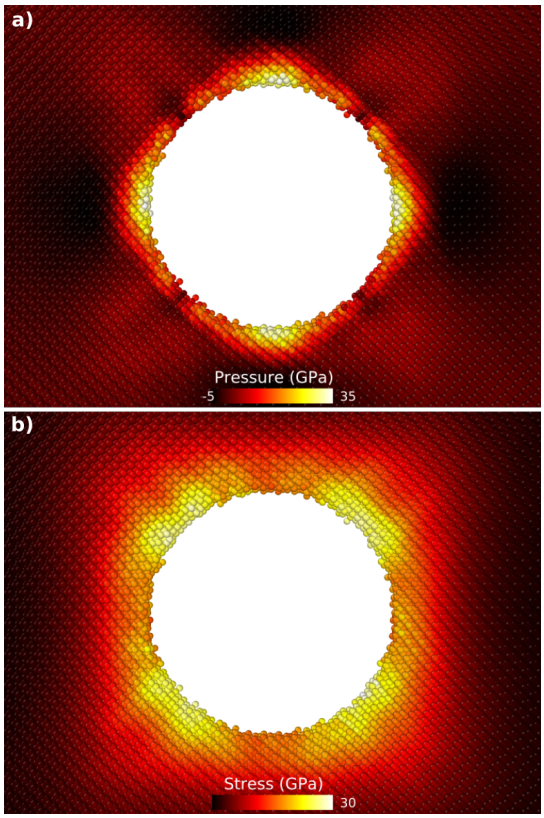

Figure 6: Atomic pressure p (a) and von Mises stress σ_{vm} (b) in the SiC matrix, for an helium-filled bubble with He/V = 6, at 10 K. For clarity, only Si/C atoms included in a 10 Å thick slice oriented along [100] are shown, and helium atoms have been removed. Note that for each atom, the displayed values of pressure and von Mises stress are spatial averages over neighboring atoms in a 6 Å sphere, as recommended for multi-component systems [58].

tion of SiC involves only partial dislocations [57].

For all cases, amorphization and dislocation nucleation occur at the bubble matrix interface, due to the combined action of stress and temperature. These mechanisms have also been identified as responsible for the plastic deformation of nano-indented SiC [59]. The pressure and the von Mises stress are shown in Fig. 6, at 10 K and He/V equal to 6, i.e. in conditions close to the onset of plastic deformation. Pressure maxima, up to 35 GPa, can be found in the vicinity of the interface, along ⟨100⟩ directions. It is obviously correlated to our previous observations on the localization of disordered regions. The computed pressure maxima are in the range of reported values associated with the amorphization of silicon carbide [60, 61].

We used von Mises stresses to estimate the shear stress magnitude associated with dislocation nucleation and propagation. Therefore our analysis is semi-quantitative, and based on the order of magnitude only. To go further would require the determination of the critical resolved shear stress that is specific for each slip systems, an excessively difficult task here given the steep stress gradients. Figure 6 shows that von Mises stress values are the highest in regions for which pressure is the lowest, with maximum values up to 30 GPa. This is seemingly not enough for forming half-loop dislocations in silicon carbide, and temperature is required to overcome the nucleation energy barrier. In fact, adding more helium in the bubbles also increases the pressure, and the SiC matrix first yields by amorphization (Fig. 4). To our knowledge, the critical stress for nucleating half-loop dislocation in SiC is an unknown quantity. A rough comparison can be made with the theoretical shear strength as given by the Frenkel model, $\sigma = \mu b/2\pi d$ [62]. With a shear modulus $\mu = 194$ GPa [63], a Burgers vector $b = 3.08$ Å and a plane spacing $d = 1.89$ Å, one obtains $\sigma \simeq 50$ GPa. On another note, first-principles calculations showed that a half-loop dislocation from a surface in silicon will nucleate when the tensile stress reaches 0.26μ [64]. It would translate to a critical stress of 50 GPa for silicon carbide. Although the agreement between the two estimations is arguably fortuitous, the order of magnitude is probably sound.

The Peierls stress associated to screw dislocations motion in SiC is 9–10 GPa [65], and a lower value is expected for non-screw leading segments. Therefore the level of stress in the vicinity of the interface is enough for dislocations to pull away from the bubble matrix interface. However, those one can not travel far, since the stress steeply decreases with the distance to the interface. This could explain why dislocations in Fig. 5 remain located close to the bubble.

5. Conclusions

In this work, we explored the properties of a nanometric helium bubble in silicon carbide for various helium densities and temperatures, motivated by the lack of similar studies for this material. Several conclusions are drawn from the analysis of molecular dynamics calculations. First there is a maximal helium density that can be reached in the bubble, the threshold value depending on the temperature. The helium density saturation is due to the plastic yielding of the silicon carbide matrix by two distinct mechanisms. The first is the amorphization of the SiC matrix in the vicinity of the bubble, that is weakly dependent on temperature. The second one implies nucleation of dislocations from the bubble matrix interface, followed by their migration over a short distance, and becomes significant at the highest temperatures. The calculated local pressure and shear stresses are in good agreement with values reported for these two mechanisms. Finally, note that our investigations focused on the 3C silicon carbide. Nonetheless, we are confident that our conclusions are also valid for common hexagonal polytypes like 4H or 6H, whose elastic and plastic properties are very close to the cubic phase [56, 57].

Recent experimental estimations of the helium density for nanometric bubbles in silicon carbide are ranging from 150 to 220 He nm^{-3} [36]. Such densities equate to calculated internal pressures betweeen 20 GPa and 60 GPa, in good agreement with common helium equation of states. Our simulations also suggest that the SiC matrix close to these bubbles is essentially elastically deformed, although a limited plastic activity cannot be fully excluded.

Finally, note that in our simulations the helium atoms are all initially present in the bubble. Although this is a standard practice in similar studies, one may wonder whether this is

Table A.1: Calculated formation energies (in eV) for different locations of a single He atom in the cubic SiC lattice: in interstitial positions (tetrahedral T_{Si}, T_C, and hexagonal H sites), in mono-vacancies (V_{Si}, V_C), and in a V_CV_{Si} di-vacancy. Third column values correspond to the results of the fit (performed using first principles data [26], reported in the second column, as a reference), whereas in the fourth column are reported the formation energies computed using the final He–Si and He–C pair potentials.

Conf.	[26]	Fit	Final
T_{Si}	3.04	3.04	3.08
T_C	3.51	3.28	3.84
H	4.53		4.20
V_{Si}	1.42	1.56	1.56
V_C	3.37	2.37	2.37
V_CV_{Si}	1.19	1.37	1.37

Table A.2: Fitted parameters for the He–C and He-Si Buckingham pair functions (eq. (A.1)).

	A (eV)	ρ (Å)	C (eV Å^6)
He–C	13.565	0.281	-6.47
He–Si	15.074	0.629	10.82

realistic compared to experiments. Introducing helium more gradually could have two effects. First the onset of plasticity may be shifted to higher helium densities. We believe that such a shift is probably small. Second, the sequences of activated plasticity mechanisms may be affected, and by extension also the final structure of the SiC matrix. Those issues could be investigated by performing molecular dynamics combined with a grand canonical Monte Carlo procedure, that would allow to introduce additional helium atoms inside an already deformed bubble. This leaves interesting prospects for future investigations.

Acknowledgements

Computations have been performed on the supercomputer facilities of the Mésocentre de calcul Poitou-Charentes.

Appendix A. He–Si–C potential

The interatomic potentials, needed for the molecular dynamics calculations, were developed according to the same guidelines than in [66]. For Si–C interactions [67], the many-body Erhart-Albe potential [67] is used. For both He–Si and He–C interactions, tabulated pair potentials are generated, starting from a Buckingham function (equation (A.1)) fitted on reference data.

$$V(r) = A\exp(-r/\rho) - \frac{C}{r^6} \qquad \text{(A.1)}$$

The A, ρ, and C parameters for He–Si and He–C pair interactions were fitted all together using first-principles calculations data as references (Table A.1). The best set of parameters is reported in Table A.2.

These pair functions are next modified in the short atomic separation regimes, for which the Buckingham potential is not accurate enough. Suitable alternatives include specific potentials like ZBL (Ziegler-Biersack-Littmark [68]) or first-principles calculations. For He–Si, we performed density functional theory calculations of a He–Si dimer with variable lengths. The computed pair energy is linked with the Buckingham potential with a 5^{th} order polynomial, in the range 1.1–1.9 Å, allowing for continuous first and second derivatives. A further refinement is made by modifying the pair potential with the ZBL potential for separations lower than 0.35 Å (also linked to the first principles calculations with a 5^{th} order polynomial in the range 0.35–0.7 Å).

We first attempted the same procedure for the He–C pair function. However, it appears that best results were obtained by only using the ZBL potential at short separations, in particular for the formation energy of a single He atom located in hexagonal interstitial. This configuration is important since it is the saddle point for the migration of He in the SiC lattice, and its corresponding energy sets the diffusion energy. Therefore, the final He–C function was obtained by linking the Buckingham potential with ZBL, using a 5^{th} order polynomial in the range 1.4–2.2 Å. The formation energies computed using these final potentials are reported in the fourth column of Table A.1.

Finally, for the He–He interactions, we used the Beck potential [69], which is well suited to describe helium for the range of density investigated in this work. This potential is connected to ZBL using a 5^{th} order polynomial in the range 0.26–0.27 Å.

Data availability

The raw/processed data required to reproduce these findings cannot be shared at this time due to legal or ethical reasons.

References

[1] G. Harris (Ed.), Properties of silicon carbide, INSPEC, Institution of Electrical Engineers, London, 1995.

[2] W. J. Choyke, G. Pensl, Physical properties of sic, Mater. Res. Soc. Bull. 22 (3) (1997) 25.

[3] P. R. Heck, K. K. Marhas, P. Hoppe, R. Gallino, H. Baur, R. Wieler, Presolar he and ne isotopes in single circumstellar sic grains, The Astrophysical Journal 656 (2007) 1208.

[4] K. Hojou, K. Izui, Bubbles in sic crystals formed by helium ion irradiation at high temperatures, J. Nucl. Mater. 160 (1988) 147.

[5] K. Hojou, S. Furuno, K. Kushita, H. Otsu, Y. Furuya, K. Izui, In situ eels and tem observation of silicon carbide irradiated with helium ions at low temperature and successively annealed, Nucl. Instrum. Methods Phys. Res. B 116 (1996) 382.

[6] J. Chen, P. Jung, H. Trinkaus, Evolution of helium platelets and associated dislocation loops in α-sic, Phys. Rev. Lett. 82 (13) (1999) 2709.

[7] E. Oliviero, A. van Veen, A. Fedorov, M.-F. Beaufort, J.-F. Barbot, Helium implantation defects in sic studied by thermal helium desorption spectrometry, Nucl. Instrum. Methods Phys. Res. B 186 (2002) 223.

[8] L. Vincent, T. Sauvage, G. Carlot, P. Garcia, G. Martin, M.-F. Barthe, P. Desgardin, Thermal behaviour of helium in silicon carbide: influence of microstructure, Vacuum 83 (2009) S36.

[9] H. Fan, R. Li, D. Yang, Y. Wu, J. Niu, Q. Yang, J. Zhao, D. Liu, Observation of he bubbles in ion irradiated fusion materials by conductive atomic force microscopy, J. Nucl. Mater. 441 (13) (2013) 54 – 58. doi:http://dx.doi.org/10.1016/j.jnucmat.2013.05.034.

[10] M.-F. Beaufort, M. Vallet, J. Nicolaï, E. Oliviero, J.-F. Barbot, In-situ evolution of helium bubbles in sic under irradiation, J. Appl. Phys. 118 (20) (2015) 205904.

[11] C.-H. Chen, Y. Zhang, Y. Wang, M. Crespillo, C. Fontana, J. Graham, G. Duscher, S. Shannon, W. Weber, Dose dependence of helium bubble formation in nano-engineered SiC at 700 °c, J. Nucl. Mater. 472 (2016) 153–160. doi:10.1016/j.jnucmat.2016.01.029.

[12] R. Harrison, S. Ebert, J. Hinks, S. Donnelly, Damage microstructure evolution of helium ion irradiated SiC under fusion relevant temperatures, J. Europ. Ceram. Soc. 38 (11) (2018) 3718–3726. doi:10.1016/j.jeurceramsoc.2018.04.060.

[13] H. Trinkaus, Energetics and formation kinetics of helium bubbles in metals, Radiation Effects 78 (1983) 189.

[14] S. E. Donnelly, The density and pressure of helium in bubbles in implanted metals: a critical review, Radiation Effects 90 (1985) 1.

[15] K. Morishita, R. Sugano, Mechanism map for nucleation and growth of helium bubbles in metals, J. Nucl. Mater. 353 (1) (2006) 52 – 65. doi:https://doi.org/10.1016/j.jnucmat.2006.03.007.

[16] G. F. Cerofolini, F. Corni, S. Frabboni, C. Nobili, G. Ottaviani, R. Tonini, Hydrogen and helium bubbles in silicon, Mater. Sci. Eng. R. 27 (2000) 1.

[17] L. Pizzagalli, M. L. David, M. Bertolus, Molecular dynamics simulation of the initial stages of he bubbles formation in silicon, Modelling Simul. Mater. Sci. Eng. 21 (6) (2013) 065002.

[18] L. Pizzagalli, J. Dérès, M.-L. David, T. Jourdan, Influence of helium on the nucleation and growth of bubbles in silicon: a multiscale modelling study, J. Phys. D: Appl. Phys. 52 (45) (2019) 455106. doi:10.1088/1361-6463/ab3816.

[19] L. V. Brutzel, A. Chartier, A new equation of state for helium nanobubbles embedded in UO2 matrix calculated via molecular dynamics simulations, J. Nucl. Mater. 518 (2019) 431–439. doi:10.1016/j.jnucmat.2019.02.015.

[20] P. Jung, Diffusion and retention of helium in graphite and silicon carbide, J. Nucl. Mater. 191-194 (1992) 377.

[21] W. R. Allen, The lattice location of helium implanted in α-sic, J. Nucl. Mater. 210 (1994) 318.

[22] P. Jung, H. Klein, J. Chen, A comparison of defects in helium implanted α- and β-sic, J. Nucl. Mater. 283-287 (2000) 806.

[23] R. M. V. Ginhoven, A. Chartier, C. Meis, W. J. Weber, L. R. Corrales, Theoretical study of helium insertion and diffusion in 3c-sic, J. Nucl. Mater. 348 (2006) 51.

[24] J. H. Kim, Y. D. Kwon, P. Yonathan, I. Hidayat, J. G. Lee, J.-H. Choi, S.-C. Lee, The energetics of helium and hydrogen atoms in β-sic: an ab initio approach, J. Mater. Sci. 44 (2009) 1828.

[25] S. Miro, J. Constantini, J. Haussy, L. Beck, S. Vaubaillon, S. Pellegrino, C. Meis, J. Grob, Y. Zhang, W. Weber, Nuclear reaction analysis of helium migration in silicon carbide, J. Nucl. Mater. 415 (2011) 5.

[26] A. Charaf Eddin, L. Pizzagalli, First principles calculation of noble gas atoms properties in 3csic, J. Nucl. Mater. 429 (13) (2012) 329 – 334. doi:http://dx.doi.org/10.1016/j.jnucmat.2012.06.022.

[27] F. Linez, F. Garrido, H. Erramli, T. Sauvage, B. Courtois, P. Desgardin, M.-F. Barthe, Experimental location of helium atoms in 6hsic crystal lattice after implantation and after annealing at 400c, Journal of Nuclear Materials 459 (0) (2015) 62 – 69. doi:http://dx.doi.org/10.1016/j.jnucmat.2014.12.118.

[28] D. Cherniak, E. Watson, R. Trappisch, J. Thomas, D. Chaussende, Diffusion of helium in SiC and implications for retention of cosmogenic he, Geochimica et Cosmochimica Acta 192 (2016) 248–257. doi:10.1016/j.gca.2016.08.007.

[29] F. Linez, E. Gilabert, A. Debelle, P. Desgardin, M.-F. Barthe, Helium interaction with vacancy-type defects created in silicon carbide single crystal, J. Nucl. Mater. 436 (13) (2013) 150 – 157. doi:http://dx.doi.org/10.1016/j.jnucmat.2013.01.288.

[30] R. Li, W. Li, C. Zhang, P. Zhang, H. Fan, D. Liu, L. Vitos, J. Zhao, Hevacancy interaction and multiple he trapping in small void of silicon carbide, J. Nucl. Mater. 457 (0) (2015) 36 – 41. doi:http://dx.doi.org/10.1016/j.jnucmat.2014.10.062.

[31] S. Zhao, G. Ran, F. Li, H. Deng, F. Gao, Ab initio study of interstitial helium clusters in 3c-SiC, J. Nucl. Mater. 521 (2019) 13–20. doi:10.1016/j.jnucmat.2019.04.027.

[32] J. Sun, B. Li, Y.-W. You, J. Hou, Y. Xu, C. Liu, Q. Fang, Z. Wang, The stability of vacancy clusters and their effect on helium behaviors in 3c-SiC, J. Nucl. Mater. 503 (2018) 271–278. doi:10.1016/j.jnucmat.2018.03.010.

[33] A. Couet, J.-P. Crocombette, A. Chartier, Atomistic study of the thermodynamic equilibrium of nano-sized helium cavities in βsic, J. Nucl. Mater. 404 (2010) 50.

[34] J. Dérès, M.-L. David, K. Alix, C. Hébert, D. T. L. Alexander, L. Pizzagalli, Properties of helium bubbles in covalent systems at the nanoscale: A combined numerical and experimental study, Phys. Rev. B 96 (2017) 014110. doi:10.1103/PhysRevB.96.014110.

[35] K. Alix, M.-L. David, J. Dérès, C. Hébert, L. Pizzagalli, Evolution of the properties of helium nanobubbles during in situ annealing probed by spectrum imaging in the transmission electron microscope, Phys. Rev. B 97 (10). doi:10.1103/physrevb.97.104102.

[36] The full details will appear in a separate publication.

[37] S. Plimpton, Fast parallel algorithms for short-range molecular dynamics, J. Comput. Phys. 117 (1) (1995) 1 – 19.

[38] S. H. Haghighat, G. Lucas, R. Schäublin, State of a pressurized helium bubble in iron, Europhys. Lett. 85 (2009) 60008.

[39] A. Abhishek, M. Warrier, R. Ganesh, A. Caro, Growth and structural determination of he bubbles in iron/chromium alloys using molecular dynamics simulations, J. Nucl. Mater. 472 (2016) 82 – 88. doi:http://dx.doi.org/10.1016/j.jnucmat.2016.02.001.

[40] A. Caro, J. Hetherly, A. Stukowski, M. Caro, E. Martinez, S. Srivilliputhur, L. Zepeda-Ruiz, M. Nastasi, Properties of helium bubbles in fe and fecr alloys, J. Nucl. Mater. 418 (1-3) (2011) 261 – 268. doi:10.1016/j.jnucmat.2011.07.010.

[41] K. Alix, M.-L. David, G. Lucas, D. T. Alexander, F. Pailloux, C. Hébert, L. Pizzagalli, Gentle quantitative measurement of helium density in nanobubbles in silicon by spectrum imaging, Micron 77 (2015) 57 – 65. doi:http://dx.doi.org/10.1016/j.micron.2015.05.011.

[42] P. Loubeyre, R. LeToullec, J. P. Pinceaux, H. K. Mao, J. Hu, R. J. Hemley, Equation of state and phase diagram of solid ^{4}he from single-crystal x-ray diffraction over a large p-t domain, Phys. Rev. Lett. 71 (14) (1993) 2272.

[43] A. Caro, D. Schwen, E. Martinez, Structure of nanoscale gas bubbles in metals, Appl. Phys. Lett. 103 (21) (2013) 213115. doi:http://dx.doi.org/10.1063/1.4833775.

[44] R. Stoller, Y. Osetsky, An atomistic assessment of helium behavior in iron, J. Nucl. Mater. 455 (13) (2014) 258 – 262, proceedings of the 16th International Conference on Fusion Reactor Materials (ICFRM-16). doi:http://dx.doi.org/10.1016/j.jnucmat.2014.06.020.

[45] A. Caro, D. Schwen, J. Hetherly, E. Martinez, The capillarity equation at the nanoscale: Gas bubbles in metals, Acta Mater. 89 (2015) 14 – 21. doi:http://dx.doi.org/10.1016/j.actamat.2015.01.048.

[46] A. Jelea, Molecular dynamics modeling of helium bubbles in austenitic steels, Nucl. Instrum. Meth. Phys. Res. B 425 (2018) 50–54. doi:10.1016/j.nimb.2018.04.008.

[47] D. Taverna, M. Kociak, O. Stéphan, A. Fabre, E. Finot, B. Décamps, C. Colliex, Probing physical properties of confined fluids within individual nanobubbles, Phys. Rev. Lett. 100 (2008) 035301.

[48] S. Fréchard, M. Walls, M. Kociak, J. Chevalier, J. Henry, D. Gorse, Study by eels of helium bubbles in a martensitic steel, J. Nucl. Mater. 393 (2009) 102.

[49] P. Mahler Larsen, S. Schmidt, J. Schiøtz, Robust structural identification via polyhedral template matching, Modelling Simul. Mater. Sci. Eng. 24 (5) (2016) 055007. doi:10.1088/0965-0393/24/5/055007.

[50] A. Stukowski, V. V. Bulatov, A. Arsenlis, Automated identification and indexing of dislocations in crystal interfaces, Modelling and Simulation in Materials Science and Engineering 20 (8) (2012) 085007.

[51] A. Stukowski, Visualization and analysis of atomistic simulation data with OVITO-the Open Visualization Tool, Modelling and Simulation in Materials Science and Engineering 18 (1). doi:10.1088/0965-0393/18/1/015012.

[52] A. Stukowski, Computational analysis methods in atomistic modeling of crystals, JOM 66 (3) (2014) 399–407.

[53] E. Maras, O. Trushin, A. Stukowski, T. Ala-Nissila, H. Jnsson, Global transition path search for dislocation formation in ge on

si(001), Computer Physics Communications 205 (2016) 13 – 21. doi:https://doi.org/10.1016/j.cpc.2016.04.001.
[54] J. Rabier, L. Pizzagalli, J.-L. Demenet, Dislocations in silicon at high stress, in: L. Kubin, J. P. Hirth (Eds.), Dislocation in solids, Vol. 16, Elsevier, 2010, Ch. 93, p. 47.
[55] D. Rodney, L. Ventelon, E. Clouet, L. Pizzagalli, F. Willaime, Ab initio modeling of dislocation core properties in metals and semiconductors, Acta Mater. 124 (2017) 633–659. doi:10.1016/j.actamat.2016.09.049.
[56] J.-L. Demenet, M. Amer, C. Tromas, D. Eyidi, J. Rabier, Dislocations in 4h- and 3c-sic single crystals in the brittle regime, Phys. Stat. Sol. (c) 10 (1) (2013) 64–67.
[57] P. Pirouz, A. V. Samant, M. H. Hong, A. Moulin, L. P. Kubin, On temperature dependence of deformation mechanism and the brittleductile transition in semiconductors, Journal of Materials Research 14 (7) (1999) 27832793. doi:10.1557/JMR.1999.0372.
[58] P. S. Branicio, D. J. Srolovitz, Local stress calculation in simulations of multicomponent systems, J. Comput. Phys. 228 (22) (2009) 8467–8479. doi:10.1016/j.jcp.2009.08.024.
[59] I. Szlufarska, R. K. Kalia, A. Nakano, P. Vashishta, Atomistic mechanisms of amorphization during nanoindentation of sic: A molecular dynamics study, Phys. Rev. B 71 (2005) 174113. doi:10.1103/PhysRevB.71.174113.
[60] M. Mishra, I. Szlufarska, Possibility of high-pressure transformation during nanoindentation of sic, Acta Materialia 57 (20) (2009) 6156 – 6165. doi:https://doi.org/10.1016/j.actamat.2009.08.041.
[61] V. I. Levitas, Y. Ma, E. Selvi, J. Wu, J. A. Patten, High-density amorphous phase of silicon carbide obtained under large plastic shear and high pressure, Phys. Rev. B 85 (2012) 054114. doi:10.1103/PhysRevB.85.054114.
[62] V. V. Bulatov, W. Cai, R. Baran, K. Kang, Geometric aspects of the ideal shear resistance in simple crystal lattices, Philosophical Magazine 86 (25-26) (2006) 3847–3859. doi:10.1080/14786430600643282.
[63] P. Djemia, Y. Roussigné, G. Dirras, K. Jackson, Elastic properties of β-sic films by brillouin light scattering, J. Appl. Phys. 95 (5) (2004) 2324.
[64] J. Godet, S. Brochard, L. Pizzagalli, P. Beauchamp, J. M. Soler, Dislocation formation from a surface step in semiconductors: An ab initio study, Phys. Rev. B 73 (2006) 092105.
[65] L. Pizzagalli, Stability and mobility of screw dislocations in 4h, 2h and 3c silicon carbide, Acta Mater. 78 (2014) 236 – 244. doi:http://dx.doi.org/10.1016/j.actamat.2014.06.053.
[66] L. Pizzagalli, Atomistic modeling of point defect contributions to swelling in xe-implanted silicon carbide, J. Nucl. Mater. 512 (2018) 349–356. doi:10.1016/j.jnucmat.2018.10.024.
[67] P. Erhart, K. Albe, Analytical potential for atomistic simulations of silicon, carbon, and silicon carbide, Phys. Rev. B 71 (2005) 035211.
[68] J. F. Ziegler, U. Littmark, J. P. Biersack, The stopping and range of ions in solids, Pergamon New York, 1985.
[69] D. Beck, A new interatomic potential function for helium, Molecular Physics 14 (4) (1968) 311–315.